HHS Public Access

Author manuscript

Biochemistry. Author manuscript; available in PMC 2020 May 29.

Published in final edited form as:

Biochemistry. 2013 December 23; 52(51): 9246–9256. doi:10.1021/bi4011495.

ATP Transport through VDAC and the VDAC–Tubulin Complex Probed by Equilibrium and Nonequilibrium MD Simulations

Sergei Yu. Noskov[*,†,§], **Tatiana K. Rostovtseva**[‡], **Sergey M. Bezrukov**[‡]

[†]Center for Molecular Simulations, Department of Biological Sciences, University of Calgary, Calgary, Alberta T2N 1N4, Canada

[‡]Program in Physical Biology, Eunice Kennedy Shriver National Institute of Child Health and Human Development, National Institutes of Health, Bethesda, Maryland 20892, United States

Abstract

Voltage-dependent anion channel (VDAC), the major channel of the mitochondrial outer membrane, serves as a principal pathway for ATP, ADP, and other respiratory substrates across this membrane. Using umbrella-sampling simulations, we established the thermodynamic and kinetic components governing ATP transport across the VDAC1 channel. We found that there are several low-affinity binding sites for ATP along the translocation pathway and that the main barrier for ATP transport is located around the center of the channel and is formed predominantly by residues in the N-terminus. The binding affinity of ATP to an open channel was found to be in the millimolar to micromolar range. However, we show that this weak binding increases the ATP translocation probability by about 10-fold compared with the VDAC pore in which attractive interactions were artificially removed. Recently, it was found that free dimeric tubulin induces a highly efficient, reversible blockage of VDAC reconstituted into planar lipid membranes. It was proposed that by blocking VDAC permeability for ATP/ADP and other mitochondrial respiratory substrates tubulin controls mitochondrial respiration. Using the Rosetta protein–protein docking algorithm, we established a tentative structure of the VDAC–tubulin complex. An extensive set of equilibrium and nonequilibrium (under applied electric field) molecular dynamics (MD) simulations was used to establish the conductance of the open and blocked channel. It was found that the presence of the unstructured C-terminal tail of tubulin in the VDAC pore decreases its conductance by more than 40% and switches its selectivity from anionic to cationic. The subsequent 1D potential of mean force (PMF) computations for the VDAC–tubulin complex show that the state renders ATP transport virtually impossible. A number of residues pivotal for tubulin binding to the channel were identified that help to clarify the molecular details of VDAC–tubulin interaction and to provide new insight into the mechanism of the control of mitochondria respiration by VDAC.

[*]**Corresponding Author:** snoskov@ucalgary.ca; Phone: 1-403-210-7971.

[§]On sabbatical leave to NICHD, NIH.

Supporting Information

Coordination numbers for ATP in the channel, individual simulations of ion current, and ROSETTA docking RMS profiles. This material is available free of charge via the Internet at http://pubs.acs.org.

The authors declare no competing financial interest.

Graphical Abstract

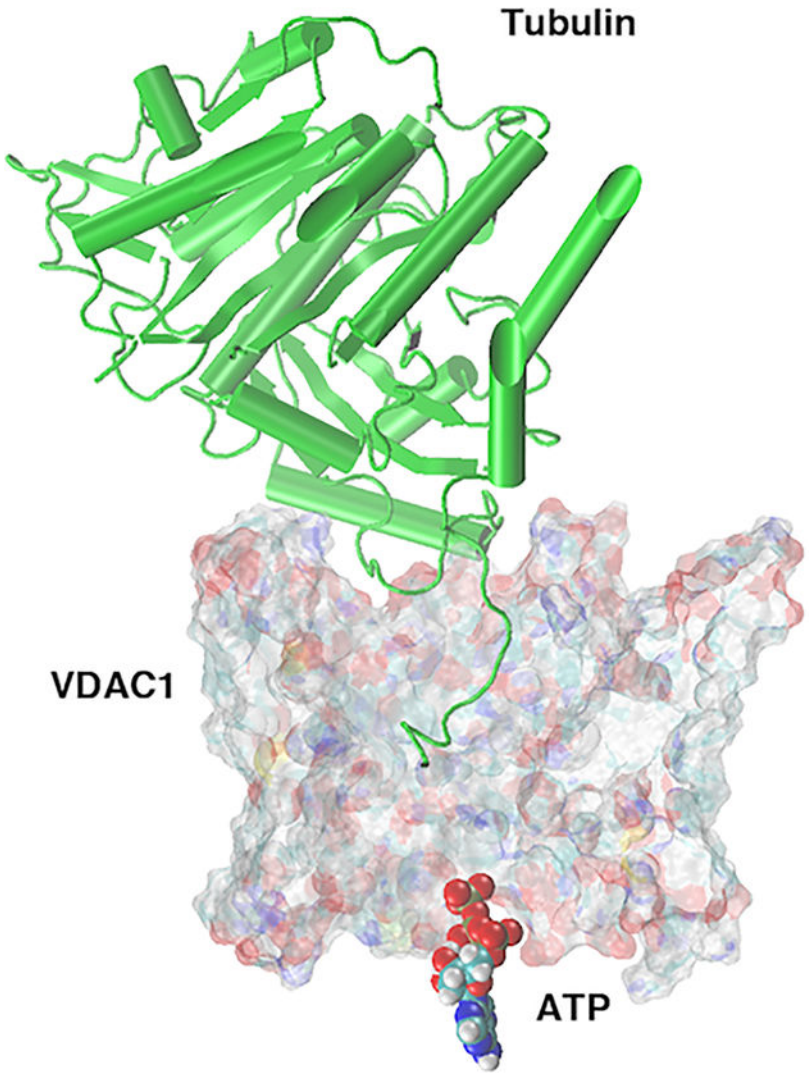

The role of mitochondria in energy production, calcium signaling, and promoting apoptosis is well-established. The fundamental question is to understand how mitochondrial functions control cell survival and death. We address this question by studying the voltage-dependent anion channel (VDAC) that constitutes the main pathway for ATP, ADP, and other mitochondrial metabolic substrates across the mitochondrial outer membrane (MOM). When reconstituted into planar lipid membrane, VDAC monomer forms a large pore permeable for uncharged poly(ethylene glycol) (PEG) up to 2000 Da[1] and to ATP.[2] The characteristic property of reconstituted VDAC is its ability under an applied voltage of >30 mV to move from a high-conducting open state to a variety of low-conducting so-called “closed” states. VDAC in its open state shows a preference for anions over cations because of the net positively charged pore interior.[3,4] The flux of ATP through open VDAC was calculated to be about 70 times less than Cl^- flux through the channel.[5] Measurements of VDAC conductance in the presence of ATP and other mono- and dinucleotides revealed a weak (in

the range of tens of millimolar) ATP binding to the VDAC pore.[6,7] The diffusion coefficient of ATP in the VDAC pore was estimated to be an order of magnitude smaller than its bulk value.[5,6] However, in spite of a few attempts,[8,9] the exact identification of the ATP binding site in VDAC remained unknown.

Recently, it was found that free dimeric tubulin induces a highly efficient, reversible blockage of VDAC reconstituted into planar lipid membranes.[10–12] Tubulin blocks ~0.6 of the open-state conductance for small ions. The blocked state has reduced dimensions compared with the open state, the selectivity is reversed from anionic to cationic, and, most importantly, it is virtually impermeable for ATP.[1] Thus, tubulin could be considered as a novel potent endogenous regulator of VDAC. These data allowed for the conclusion that by blocking VDAC permeability tubulin could control fluxes of ATP, ADP, and other respiratory substrates across MOM and thus regulate mitochondrial respiration. Experiments with isolated mitochondria[12,13] and with intact cancer cells[14,15] support this assumption. A model of VDAC–tubulin interaction was suggested where the negatively charged C-terminal tail (CTT) of tubulin permeates into the channel lumen and reversibly blocks the channel in a highly voltage-dependent manner.[10–12]

It was also found recently that the VDAC–tubulin interaction is extremely sensitive to the state of VDAC phosphorylation by serine/threonine kinases.[16] VDAC phosphorylation increased the on-rate of VDAC–tubulin binding about 100 times, but it did so at the cis side of the channel only (the cis side has been defined as the side of VDAC addition[16]). These results allowed for the identification of the reconstituted VDAC orientation in the planar lipid membrane and suggested that the extramembrane loops opposite to the C-terminal end face the cytosolic side of the channel.[16] This conclusion was supported by DePinto et al.[17] who reported that the C-terminus is not accessible for cleavage by cytosolic caspases in permeabilized HeLa cells with expressed human VDAC1. In spite of the rapidly accumulating data on the VDAC–tubulin interaction, the exact structure of the VDAC–tubulin complex and mechanism of tubulin binding to the VDAC pore on the level of individual residues have yet to be tested and established.

Here, we use molecular dynamic (MD) simulations to address questions about structural arrangements of the VDAC–tubulin complex and to identify the residues that are responsible in creating the steric and electrostatic wells and barriers for ATP translocation through VDAC. First, using umbrella-sampling simulations, we found several low-affinity binding sites for ATP along its translocation pathway through the VDAC1 pore, with the main barrier for ATP transport located near the pore center and formed predominantly by residues in the VDAC N-terminus. The binding affinity of ATP to the open channel was found to be in the micromolar to millimolar range, which correlates nicely with the weak ATP binding found previously by electrophysiological methods.[5–7] Importantly, although weak, these attractive interactions increase the efficiency of VDAC-facilitated ATP transport by about 10-fold compared with the channel in which only steric interactions are kept conserved. Second, using the Rosetta protein–protein docking algorithm, we established a tentative structure of the VDAC–tubulin complex that allowed calculation of the conductances of the open and tubulin-blocked channel states. We found that the unstructured C-terminal tail of α-tubulin switches VDAC1 selectivity from anionic to cationic, as was shown

experimentally with reconstituted channels.[1,12] The subsequent 1D potential of mean force (PMF) computations for the VDAC–tubulin complex showed that the presence of the CTT tail in the channel renders ATP transport virtually impossible. This result is in accordance with previous direct measurements of ATP partitioning into VDAC where tubulin was shown to nearly completely prohibit ATP from entering the channel.[1] Taken together, our MD simulation data support the earlier suggested model of the VDAC–tubulin interaction where tubulin CTT partially blocks the VDAC pore, reverses its selectivity, and obstructs ATP transport. Our results provide a key to new ventures in targeting specific residues essential for the VDAC–tubulin interaction and hence for the control of mitochondrial respiration. Considering that most of tubulin post-translational modifications occur on its CTT,[18] the structural mechanisms described in this article offer a testable hypothesis of the effects of tubulin post-translational modifications on the regulation of VDAC permeability.

METHODS

MD Simulations.

Structures of the VDAC1 channel[19] and α-tubulin[20] were taken from the X-ray coordinates deposited at PDB under accession codes 3EMN and 1TVK, respectively. The α-tubulin structure contained its C-terminus, as reported by Freedman et al.[21] The simulation systems for the VDAC1 channel and VDAC1–tubulin complex were constructed using the web-based CHARMM-GUI membrane builder.[22] The simulation box contained one protein or a single complex embedded into a 1-palmitoyl-2-oleoyl phosphatidylethanolamine (POPE) bilayer and was solvated by 1 M KCl in an aqueous solution. The simulations box contained ~75 000 atoms for VDAC and VDAC-ATP systems and ~210 000 atoms for the VDAC–tubulin complex. Each system was equilibrated at 303.15 K with NPAT ensemble for 10 ns using periodic boundary conditions and particle mesh Ewald (PME) summation for long-range electrostatic interactions. This was followed with production runs of 50 ns. The temperature was maintained using a Lowe–Anderson thermostat as implemented in NAMD2.9 by Wells and Aksimentiev.[23] The van der Waals interactions were switched off at 14–16 Å by a force-switching function.[24] Long-range electrostatic interactions were calculated using the PME method, with a grid spacing of 0.75 Å for fast Fourier transformation, $\kappa = 0.34$ Å^{-1}, and a sixth-order B-spline interpolation.[25] All bond lengths involving hydrogen atoms were fixed using SHAKE to enable a 2 fs time step.[26]

The fully equilibrated protein–membrane–solvent systems were used to compute ion conductance. The constant electric field corresponding to a potential drop of 1 V was applied across the system. The stepwise protocol of Wells et al. was used for all simulations.[23] It has been tested for a variety of systems and has shown excellent performance.[27,28] The production runs to assess conductance were performed in NVT ensemble as described previously.[23] All of the simulations with applied voltage were run for 50 ns. To assess the distribution of open-pore conductances from nonequilibrium MD simulations, we ran five separate simulations similar to techniques used before.[29–32] The uncertainty in the currents computed for the tubulin-blocked state were estimated from block-averaging over the last 25 ns of the simulations with applied voltage. All MD simulations were performed with program suite NAMD ver2.9.[33] Subsequent analysis of the system was done using the

CHARMM program suite (35b1r1).[34] The CHARMM27 force field with cross-term map (CMAP)[34] corrections were used for proteins, and CHARMM-36 parameters were used to represent lipids.[35] The rigid TIP3P model represented the solvent.[36]

Protein–Protein Docking with RosettaDock.

We used RosettaDock to obtain initial structures for the VDAC1–tubulin complexes. It employs a Monte Carlo (MC) search with low-resolution runs followed by high-resolution refinements. The details of the docking scheme are described elsewhere.[37,38] Twenty different starting orientations of tubulin with respect to VDAC were generated for the subsequent docking runs. The docking protocol started with 15 000 steps of a low-resolution rigid-body MC search followed by 500 cycles of refinement. The docked structures were clustered to produce four different starting complexes for MD simulations. The subsequent analysis of simulations shows that the bound tubulin orientation is virtually the same in all four starting complexes after 10 ns of equilibration.

Umbrella-Sampling Simulations and WHAM Analysis.

Umbrella-sampling simulations for ATP transport across open VDAC1 and VDAC1–tubulin systems were carried out using the NAMD program.[39] Harmonic constraints of 10 kcal/(mol· Å^2) were applied to the reaction coordinate spanning 60 Å across the channel. The 1D solute transport reaction coordinate was initially defined along the central axis of the channel. The cylindrical constraint with a radius of 20 Å was applied to the ATP molecule to ensure that the computed PMF is bounded. We used 120 windows spaced every 0.5 Å to describe ATP transport along the channel. Umbrella-sampling simulations were performed with harmonic biasing potentials with a force constant of 10 kcal/(mol·Å^2) along the channel axis, z axis. The zero position along the z axis coincides with the center of mass of the backbone atoms of VDAC1.

The generation of the initial windows for sampling ATP dynamics in the channel represents a significant challenge because of the size, charge, and flexibility of the substrate.[40] We adopted the following strategy tested previously for generating the initial path. The PMF windows were generated by running six independent targeted MD simulations[41] as implemented in CHARMM.[34] We generated the starting orientations of substrate for each of the TMD runs by applying random rotations to the ATP molecule while keeping the center of mass restrained at the desired position. The details of the TMD runs were published previously.[42] The starting conformations for each of the US runs were extracting by k-means clustering analysis. Each window was equilibrated for 2.5 ns in the presence of a restraining potential and then subjected to a 5 ns production run that was used for weighted histogram analysis (WHAM).[43] The WHAM convergence tolerance was set at 0.00001 kcal/mol. The statistical uncertainties were estimated by separating the data into seven blocks. The binding constant for a substrate in the presence of cylindrical constraints can be defined as[44,45]

$$K_{\mathrm{b}} = \pi R^2 \int_{z_{\mathrm{left}}}^{z_{\mathrm{right}}} \mathrm{d}z \exp(-W(z)/k_{\mathrm{B}}T) \quad (1)$$

where k_B and T have their usual meaning of the Boltzmann constant and absolute temperature, respectively, and R is the radius of the cylindrical restraint oriented normal to the z axis in which $z_{left} = -30$ Å and $z_{right} = 30$ Å. The $W(z)$ was offset to zero when the ATP molecule moves to the mitochondrial intermembrane side. The radius of the cylindrical confinement was large enough to allow for lateral dynamics of a substrate and exceeds the radius of the pore.[46,47]

MM-PBSA Computations of Binding Enthalpies for VDAC–Tubulin Complexation.

Enthalpies of VDAC–tubulin complexation were computed as averages from an ensemble of structures (1000 frames) sampled from evenly distributed points over the last 20 ns of the production runs. The electrostatic contribution to binding was obtained by solving a linearized version of the Poisson–Boltzmann equation as implemented in the PBEQ module of CHARMM.[48,49] A dielectric constant of 2 was assigned to the protein, and the protein–solvent surface was defined using the set of optimized atomic radii from Nina et al.[48] Following the numerical recipe of Chandra et al.,[50] the membrane was represented by a 24 Å slab of low dielectric 2. The focusing method was used to solve the PB equation with a coarse grid spacing of 1.5 Å and fine grid spacing of 0.5 Å. Protein–ligand complex occupied ~80% of the grid volume. The nonelectrostatic components of binding enthalpies were represented with scaled LJ terms as described by Swanson and McCammon.[51]

RESULTS AND DISCUSSION

Free-Energy Profile for ATP Transport Across the Open VDAC Channel.

To unravel the energetics of ATP permeation, we employed umbrella-sampling methods, a powerful computational technique used with considerable success in studies of membrane proteins.[44,46,52] The resulting PMF for ATP transport is shown in Figure 1 along with the pore radius. Although the errors for the computed PMF profile are significant, it is still possible to identify binding sites and location of the barrier. From the 1D PMF, an ATP molecule shows a well-pronounced binding site located $-3 < z < -12$ Å (state 1 in Figure 1, black symbols) and then another, shallower binding site at $10 < z < 18$ Å (state 3). The exact locations of the minima are $z = -10.7$ and 13.6 Å for states 1 and 3, respectively. The two tentative binding locations are separated by a small barrier (state 2), with the peak at $z = 4.2$ Å. The presence of a shallow minimum for a binding sites spanning over several angstroms is not surprising. It has to accommodate a well-hydrated and flexible ligand such as ATP. Similar behavior was observed before for PMF computations for protein–protein[53] and protein–ligand association.[54,55]

The deepest energy well (state 1) for ATP is approximately −6.5 kcal/mol. The dissociation constant for ATP estimated from eq 1 is ~125 μM, which is in reasonable agreement with the experimentally measured millimolar binding affinity[6,7] for a ligand as large as ATP. The most favorable site for ATP in the channel is in general agreement with the proposed location of a binding site around the middle of the channel.[7,56]

As was analytically considered elsewhere,[57–59] solute-channel binding with optimal strength and distribution can greatly improve channel efficiency even for passive, concentration-

gradient-driven diffusion. The mechanism of this improvement is that the optimal binding is able to compensate for the entropy cost of moving a solute molecule through the confines of the channel. If we accept a proposed orientation of the channel in the outer membrane with the C-terminus facing the mitochondrial intermembrane space,[16,17] then the z coordinate along the channel at +30 Å in the graph in Figure 1 would correspond to the cytosolic side of the channel, and at −30 Å, to the mitochondrial side. The barrier to escape the binding well around the middle of the channel to the mitochondrial side is $6k_BT$, whereas the barrier to overcome for transport from the second binding site to the cytosolic side is ~$4k_BT$. The pore radius shown in Figure 1 (red symbols) provides some explanations for the observed asymmetry of the PMF. The constriction zone formed by the helical structure in the N-terminus is shifted toward the cytosolic side. The asymmetric pore profile combined with the asymmetry in the charge distribution on the channel surface results in two different ATP binding sites.

To understand better the structural organization of the binding site for ATP and the nature of the barrier, we performed per-residue decomposition of ATP-binding enthalpies for the umbrella windows that correspond to the locations of the binding sites (state 1 and state 3) and barrier (state 2). The results are collected in Figure 2A,B. Figure 2A shows that the translocating ATP molecule relies on electrostatic interactions with the residues located predominantly in the VDAC N-terminus. MD simulations suggest that the helix-break-helix motif of the N-terminus (residues 6–23) is very stable in the course of the simulations. The unstructured N-terminal tail (residues 1–5) is flexible and can reach out of the channel lumen to either the cytosolic or mitochondrial intermembrane space.

The data collected in Figure 2A and illustrated in Figure 2B show that four negative charges of the bound ATP molecule are stabilized by two to three basic side chains (K12, R15, and K20) of VDAC and two to three counterions (Supporting Information Figure 1). The coordination-occupancy analysis shows that the flexible side chains of K12 and K20 form salt bridges with ATP in ~65% of all frames, whereas in the rest of the trajectories these side chains are involved in water-mediated stabilization of the ATP molecule (Supporting Information Figure 1). While ATP moves deeper into the channel, it has to break these stabilizing interactions. The per-residue decomposition of binding enthalpies for state 2 (barrier) in PMF shows a decrease in favorable interactions between the ATP molecules and the two key basic residues located on N-terminus (i.e., K12 and K20). The location of the barrier in PMF also coincides with a constriction zone reflected in a considerable decrease in the pore radius (Figure 1). The second binding site located near the cytosolic entrance is formed by two basic residues from β-sheets (K53 and K113) and N55, which stabilizes the nucleobase of adenosine. The repulsive interactions with D78 destabilize the binding of ATP to this site. The previously found lower affinity of VDAC for ADP and AMP than for ATP[7] can be rationalized in terms of electrostatic matching. The data collected in Figure 2A shows that salt-bridging interactions between basic residues of VDAC and phosphates of ATP are the key determinants for stable binding, and missing a single phosphate would inhibit it. Interestingly, on the basis of the studies of K20S mutant VDAC1, the N-terminus and especially residue K20 have been identified as an ATP binding site,[8] which supports our findings nicely.

The obtained profiles of the PMF of ATP translocation together with the pore radius along the z axis have allowed us to evaluate the channel efficiency analytically. Using the data plotted in Figure 1, we compared the translocation probabilities in two cases: the probability, P_{PMF}, calculated for an ATP molecule experiencing the action of the PMF $W(z)$ shown by black circles and the probability, P_{Ent}, calculated when the attractive interactions between the channel and ATP are switched off so that the only component of the potential is the entropic one because of the radius variations $R(z)$ shown as red circles. Our considerations are based on the continuum diffusion model of channel-facilitated transport.[57–59] It was shown that the translocation probability for a particle at the channel entrance in the case of an unbiased empty channel with entrances of equal radii R on both sides of the membrane can be estimated as (see formula 4.4 of ref[58])

$$P = \frac{1}{2 + \frac{4D_b}{\pi R}\int_{z_{left}}^{z_{right}} dz \frac{\exp(W(z)/k_B T)}{D(z)}} \quad (2)$$

where D_b and $D(z)$ in our case are the ATP diffusion coefficients in the bulk and inside the channel, respectively. The effective diffusion coefficient of ATP in the VDAC pore was estimated to be an order of magnitude smaller than in the bulk;[5,6] however, such an effective coefficient, deduced from the average residence time of ATP in the channel, necessarily includes contributions from the attractive interactions demonstrated by the present study.

Assuming $D(z)$ to be position-independent and equal to half of that in the bulk, $D_b/D(z) = 2$, and taking $W(z)$ values from Figure 1 (prorated by a factor of 0.592^{-1} to go from kcal/mol units to $k_B T$ per molecule units at room temperature) in the $-25 < z < 25$ Å range and $R_{left} \simeq R_{right} = 20$ Å, we obtain $P_{PMF} \approx 0.43$. To calculate P_{Ent}, that is the translocation probability of ATP through the VDAC channel at the switched-off attractive interactions, we used the $R(z)$ dependence given in Figure 1 and the following expression for $W(z)$

$$W(z) = W_{Ent}(z) = -2k_B T \ln(R(z)/R) \quad (3)$$

Equation 2 then gives an estimate $P_{Ent} \approx 0.045$, which is predictably small. Indeed, to translocate, the APT molecule has to climb a significant entropic barrier because of the decreasing radius. Thus, attractive interactions found in the molecular dynamics simulations of the present study increase the probability of ATP translocation through the channel by $P_{PMF}/P_{Ent} \simeq 9.7$ times. It should be noted that the length of the channel along the z coordinate that we used for this estimation exceeds that of the resolved crystal structure to account for the finite size of the ATP molecule. If we limit the channel length to the smaller $-20 < z < 20$ Å range (correspondingly, $R_{left} \simeq R_{right} = 15$ Å, see Figure 1), then the ratio of probabilities turns out to be approximately conserved. Notably, notwithstanding this significant gain in efficiency, the binding constant reflects the relatively weak interaction of ATP with the channel.

Analysis of the coordination shell of ATP in the bulk and in the channel suggests that substrate remains fully hydrated with a small drop in hydration from ~34 to ~29 water molecules. The average coordination numbers as functions of the ATP position in the

channel are shown in Supporting Information Figure 1. The average number of counterions for the ATP molecule changes from $N_{K+} \sim 4$ to $N_{K+} \sim 2.3$ upon entering the channel. The energetic penalty for the drop in counterion pairing to ATP is compensated by interactions with two basic side chains of K12 and K20. Chloride anions, as expected, are not involved in the coordination of ATP molecules either in the bulk or inside the channel.

VDAC–Tubulin Complex.

The summary for the RosettaDock rigid-body docking simulation results are collected in Supporting Information Figure 2. We used distance-based exclusion criteria to reduce conformational sampling only for poses prohibiting complexation between VDAC and α-tubulin in a membrane phase. Available experimental data suggest membrane surface localization of tubulin binding,[60] and recent MD simulations support it (unpublished). The docking results show a funnel-like dependence of the binding energy on IRMS criteria developed by Wang et al.[61] Although it is expected for a successful docking run to produce funnel-like plot, we decided to run equilibrium MD simulations to refine the complex structure. Notably, all of the low-energy poses display formation of a complex interface between VDAC and tubulin that involves tubulin C-terminus penetration into the channel lumen. The rms values for the backbone of tubulin and VDAC for simulations with a free channel and the complex are shown in Supporting Information Figure 2. The rms fluctuations plateau at ~3 to 4 Å relative to the original crystal structures of monomers and at ~4.5 to 6 Å relative to the entire complex. It is important to stress that rms values obtained in this work are in the range expected from stable protein dynamics. Analysis of B factors (not shown) suggests the C-terminus of tubulin to be the most dynamic element of the complex (Figure 3A).

To investigate the contact surface between VDAC and tubulin, we extended MM-PBSA computations for the tubulin-binding enthalpy and its decomposition into per-residue contributions. The results of the per-residue decomposition are collected in Figure 3B,C. It was found that one of the α-tubulin α-helixes (residues K336 and C347) interacts extensively with one of the cytosolic loops of VDAC1. The most stable contacts are formed between K336 of tubulin and D186 of VDAC positioned on the cytosolic loop (Figure 3A). Although the per-residue contribution from D186 is unfavorable for binding because of the high desolvation penalty, the sum of the two terms (D186 from VDAC and K336 from tubulin) is favorable for VDAC–tubulin complexation. Interestingly, on the basis of the results with the reconstituted VDAC, it was suggested that in addition to CTT binding to the pore interior there is another binding site(s) between the tubulin main body (“tail-less” protein) and the VDAC extracellular loops that form the channel entrance.[11,12,16] This conclusion was supported by two lines of experimental results:(1) tubulin with proteolitically cleaved CTT, tubulin-S, induced high-frequency current noise that is a reliable indication of its interaction with the channel[12] and (2) phosphorylation of VDAC increased the on-rate of tubulin binding, whereas the off-rate and properties of the open single channels were not altered by phosphorylation.[16]

The C-terminus of tubulin forms stable salt bridges with the N-terminus of VDAC1. The negatively charged C-terminus is accommodated by the VDAC pore providing matching

basic residues that form stable salt bridges such as between E445 to E450 of tubulin and R15, K20, K12, K28, and K32 of VDAC. Three of the identified VDAC basic residues are located in the N-terminus. K28 and K32 are located on the adjacent β-sheets, creating a ring of basic residues around the constriction zone. The favorable salt bridging is modulated by a number of repulsive interactions with the acidic side chains located on β-sheets of VDAC including D30, E59, and E280.

Tubulin Modulation of VDAC Conductance.

To test the effect of the tubulin C-terminal tail on ion conductance of VDAC1 channel, we first computed the conductance in the presence of a constant electrical field corresponding to a potential drop of 1 V. To determine ion currents, we used ion coordinates collected every 5 ps over the last 25 ns of the trajectories. At an arbitrary time, t, the instantaneous current can be expressed as[23,62]

$$I(t) = \frac{1}{\Delta t L_z} \sum_{1}^{N} q_i [z_i(t + \Delta t) - z_i(t)] \quad (4)$$

where L_z is the length of the channel along the z axis and z_i and q_i are the z coordinate and the charge of atom i, respectively.

To avoid systematic errors resulting from drift of the system, all of the frames were reoriented using crystal structure as a reference. The results of the MD runs are collected in Figure 4A,B for MD simulations with the tubulin-bound and tubulin-free states of VDAC1, respectively. The standard errors in the computed currents were estimated from five separate MD runs of 20 to 50 ns each (current traces for open-state VDAC simulations are shown in Figure S3). The open-pore conductance for all of the studied systems varied from 4.4 to 5.6 nS and displayed a weak preference for anions. The conductance is overestimated compared to the experimental measurements, but MD simulations under an applied field display a notable dependence in the computed conductances on the choice of the ion force field.[23] Although estimation of channel selectivity from simulations in symmetric salt provides only qualitative data,[63,64] the results are in general agreement with experiments on the open-state currents through VDAC and previous MD simulations studies of VDAC1.[64,65]

The binding of tubulin results in a reduction of the volume available for permeation as well as neutralization of some of the positive charges on the channel surface because of the formation of salt bridges between tubulin CTT and VDAC residues. Although the average conductance of the VDAC open state of 5.0 ± 0.27 nS is somewhat higher than that measured in the electrophysiological experiments (4.1 ± 0.1 nS in 1 M KCl[4,11,12]), the ratio between the conductance of tubulin-blocked and open state of ~0.58 is in qualitative agreement with the data obtained in the channel-reconstitution experiments.[11,12] The binding of tubulin leads to a drop in monovalent ion VDAC conductance to ~0.58 of its tubulin-free value and to the reversal of channel anionic selectivity to cationic. The simulations run for the complex suggest a K^+/Cl^- ratio of ~1.4, whereas for the open channel, this ratio is ~0.7. These numbers are reasonably close to those experimentally

obtained for the tubulin-blocked and VDAC open states, $P_K/P_{Cl} = 2.4 \pm 0.7$ and 0.5 ± 0.02, respectively.[12]

The averaged numerical densities of counterions are collected in Figure 4C. The presence of the α-tubulin CTT in the VDAC1 pore causes a significant perturbation in the densities of K^+ and Cl^- inside the channel (solid lines) compared to that in the open VDAC (symbols). The density of Cl^- is moderately depleted at or around cytosolic entrance ($20 < z < 30$ Å) where tubulin binds compared with the tubulin-free state. This reflects that CTT causes electrostatic repulsion, making Cl^- entrance into the pore more difficult. A relatively modest decrease in Cl^- density suggests that all of the charges on tubulin's CTT are well-screened by the solvent. At the same time, the density of K^+ displays a well-pronounced peak around the position of K20 in the complex, a feature not present in the open VDAC channel (Figure 4C).

K20/R15 was found to be essential for tubulin binding to VDAC1. The tubulin C-terminus shows significant conformational dynamics and forms a number of short-lived contacts with VDAC residues, but it almost always remains coordinated by either basic residues or mobile counterions, which may explain the peak in K^+ density in Figure 4C. Figure 5 displays the average electrostatic maps of the VDAC–tubulin complex (Figure 5A) and open VDAC (Figure 5B). The corresponding average electrostatic profiles along the symmetry axis of the VDAC pore are shown in Figure 5C. These maps were computed by averaging instantaneous solutions of the Poisson equation over the entire MD trajectories sampled every 5 ps as described by Aksimentiev and Schulten.[62] Away from the lipid membrane and the protein, the potential is uniform, as expected for the bulk solution. The potential drop across VDAC is smooth, without well-pronounced nonuniformities (black symbols in Figure 5C). The binding of tubulin introduces a significant perturbation in the potential across the channel on the cytosolic side of the channel ($35 < z < 0$ Å, red symbols) and around the outer surface, in good agreement with the observed CTT penetration in the VDAC1 permeation pathway and localization of charged side chains on the contact surface of α-tubulin. In the simulation set up, bound α-tubulin occupies a significant volume of the simulation cell, expectably perturbing the computing of the electrostatic profile of the system. α-Tubulin has a slightly acidic protein body that contributes to the potential profile, extending it far beyond the channel entrance up to an additional 40 Å along globular tubulin. An increase in a net negative charge because of the presence of tubulin is also expected to contribute to the observed modification of channel ion selectivity.

ATP Transport Across VDAC–Tubulin Complex.

The main role of VDAC is to provide a pathway for ATP across the mitochondrial outer membrane. Therefore, what is important is to probe the permeability of the tubulin-blocked state for ATP. To ascertain how binding of tubulin affects ATP permeation, we computed 1D PMF for ATP translocation through the pore in the presence of the tubulin CTT (Figure 6). We used the same strategy as described before for the evaluation of ATP transport across the open VDAC channel. Our PMF was capped at $z = -35$ Å and $z = 0$ Å, and ATP dynamics were bounded by a cylindrical restraint. Extending the PMF further toward the cytosolic side of the channel was found to be challenging because of steric clashes between the restrained

ATP molecule and bound α-tubulin. The computed PMF for the tubulin-bound state reveals a striking, yet expected, difference. The presence of the negatively charged CTT of tubulin prevents ATP binding to the most stable state inside the channel (state 1 in Figure 1). The barrier for ATP translocation to that binding site because of the presence of the CTT in the pore is ~2–3 kcal/mol, which is in accord with a strong electrostatic repulsion between the ATP molecule and the negative charges on the CTT and significant pore hydration. Unlike small mobile anions like Cl^-, the bulkier ATP molecule causes significant steric clashes with the bound tubulin. The tubulin CTT protruding through the pore binds to the VDAC positive residues (K12, R15, K20, K28, K32, and K256), rendering them unavailable to interactions with ATP molecules. These results are in a good agreement with the previously shown inability of ATP to partition into the tubulin-blocked state obtained in single-channel experiments.[1]

CONCLUSIONS

The results of MD simulations of ATP transport through the open VDAC and its tubulin-blocked state are in good agreement with the data obtained in channel-reconstitution experiments, thus opening the possibilities for further analysis of transport of other physiologically important nucleotides and mitochondrial metabolites through the open and tubulin-blocked VDAC pore. The computed dissociation constant for ATP binding to VDAC is ~125 μM, which is in reasonable agreement with experimental measurements and places ATP binding to VDAC in the micromolar to millimolar range. There are two distinct ATP binding sites in VDAC: one in the middle of the pore where the N-terminus forms a constriction zone and another near the presumably cytosolic entrance of the channel. For the first time, we report a model of the VDAC–tubulin complex from Rosetta docking and refinements with MD simulations. We found that the tubulin CTT protrudes through the VDAC pore and forms stable salt bridges predominantly with the VDAC N-terminus. The VDAC–tubulin complex shows decreased conductance and reversed selectivity in comparison with the open state. The tubulin–VDAC complex is virtually impermeable to ATP because of the high electrostatic and steric barriers created by the presence of the tubulin CTT.

Supplementary Material

Refer to Web version on PubMed Central for supplementary material.

ACKNOWLEDGMENTS

We thank Jack Tuszynski, Holly Freedman, and Tyler Luchko for sharing the coordinates for the refined model of α-tubulin with a C-terminal tail and for their fruitful discussion of it.

Funding

This work was supported with intramural funding from NICHD and the National Sciences and Engineering Research Council (discovery grant RGPIN-315019 to S.Y.N.). S.Y.N. is an Alberta Innovates Technology Futures New Faculty, Canadian Institute for Health Research New Investigator, and an Alberta Innovates Health Solutions Scholar. Computations were performed on the West-Grid/Compute Canada facilities and the University of Calgary TNK cluster supported by the Canadian Foundation for Innovation.

REFERENCES

(1). Gurnev PA, Rostovtseva TK, and Bezrukov SM (2011) Tubulin-blocked state of VDAC studied by polymer and ATP partitioning. FEBS Lett. 585, 2363–2366. [PubMed: 21722638]

(2). Rostovtseva T, and Colombini M (1996) ATP flux is controlled by a voltage-gated channel from the mitochondrial outer membrane. J. Biol. Chem 271, 28006–28008. [PubMed: 8910409]

(3). Blachly-Dyson E, Peng SZ, Colombini M, and Forte M (1990) Selectivity changes in site-directed mutants of the VDAC ion channel – structural implications. Science 247, 1233–1236. [PubMed: 1690454]

(4). Colombini M, Blachly-Dyson E, and Forte M (1996) VDAC, a channel in the outer mitochondrial membrane, in Ion Channels (Narahashi T, Ed.) pp 169–202, Plenum Press, New York.

(5). Rostovtseva T, and Colombini M (1997) VDAC channels mediate and gate the flow of ATP: Implications for the regulation of mitochondrial function. Biophys. J 72, 1954–1962. [PubMed: 9129800]

(6). Rostovtseva TK, and Bezrukov SM (1998) ATP transport through a single mitochondrial channel, VDAC, studied by current fluctuation analysis. Biophys. J 74, 2365–2373. [PubMed: 9591663]

(7). Rostovtseva TK, Komarov A, Bezrukov SM, and Colombini M (2002) Dynamics of nucleotides in VDAC channels: Structure-specific noise generation. Biophys. J 82, 193–205. [PubMed: 11751308]

(8). Yehezkel G, Abu-Hamad S, and Shoshan-Barmatz V (2007) An N-terminal nucleotide-binding site in VDAC1: Involvement in regulating mitochondrial function. J. Cell. Physiol 212, 551–561. [PubMed: 17503466]

(9). Yehezkel G, Hadad N, Zaid H, Sivan S, and Shoshan-Barmatz V (2006) Nucleotide-binding sites in the voltage-dependent anion channel: Characterization and localization. J. Biol. Chem 281, 5938–5946. [PubMed: 16354668]

(10). Rostovtseva TK, and Bezrukov SM (2008) VDAC regulation: Role of cytosolic proteins and mitochondrial lipids. J. Bioenerg. Biomembr 40, 163–170. [PubMed: 18654841]

(11). Rostovtseva TK, and Bezrukov SM (2012) VDAC inhibition by tubulin and its physiological implications. Biochim. Biophys. Acta, Biomembr 1818, 1526–1535.

(12). Rostovtseva TK, Sheldon KL, Hassanzadeh E, Monge C, Saks V, Bezrukov SM, and Sackett DL (2008) Tubulin binding blocks mitochondrial voltage-dependent anion channel and regulates respiration. Proc. Natl. Acad. Sci. U.S.A 105, 18746–18751. [PubMed: 19033201]

(13). Monge C, Beraud N, Kuznetsov AV, Rostovtseva T, Sackett D, Schlattner U, Vendelin M, and Saks VA (2008) Regulation of respiration in brain mitochondria and synaptosomes: Restrictions of ADP diffusion in situ, roles of tubulin, and mitochondrial creatine kinase. Mol. Cell. Biochem 318, 94–1562.

(14). Maldonado EN, Patnaik J, Mullins MR, and Lemasters JJ (2011) Free tubulin modulates mitochondrial membrane potential in cancer cells. Cancer Res. 70, 10192–10201.

(15). Maldonado EN, Sheldon KL, DeHart DN, Patnaik J, Manevich Y, Townsend DM, Bezrukov SM, Rostovtseva TK, and Lemasters JJ (2013) Voltage-dependent anion channels modulate mitochondrial metabolism in cancer cells regulation by tubulin and erastin. J. Biol. Chem 288, 11920–11929. [PubMed: 23471966]

(16). Sheldon KL, Maldonado EN, Lemasters JJ, Rostovtseva TK, and Bezrukov SM (2011) Phosphorylation of voltage-dependent anion channel by serine/threonine kinases governs its interaction with tubulin. PloS One 6, e25539–1–e25539–10. [PubMed: 22022409]

(17). Guarino F, Tomasello MF, Magri A, Impellizzeri A, Reina S, Messina A, and De Pinto V (2013) VDAC1 topology in the outer mitochondrial membrane: The final answer. Biophys. J 104, 539A–540A.

(18). Westermann S, and Weber K (2000) Cloning and recombinant expression of the La RNA-binding protein from Trypanosoma brucei. Biochim. Biophys. Acta, Gene Struct. Expression 1492, 483–487.

(19). Ujwal R, Cascio D, Colletier JP, Faham S, Zhang J, Toro L, Ping PP, and Abramson J (2008) The crystal structure of mouse VDAC1 at 2.3 angstrom resolution reveals mechanistic insights into metabolite gating. Proc. Natl. Acad. Sci. U.S.A 105, 17742–17747. [PubMed: 18988731]

(20). Nettles JH, Li HL, Cornett B, Krahn JM, Snyder JP, and Downing KH (2004) The binding mode of epothilone A on alpha,beta-tubulin by electron crystallography. Science 305, 866–869. [PubMed: 15297674]

(21). Freedman H, Luchko T, Luduena RF, and Tuszynski JA (2011) Molecular dynamics modeling of tubulin C-terminal tail interactions with the microtubule surface. Proteins 79, 2968–2982. [PubMed: 21905119]

(22). Jo S, Kim T, and Im W (2007) Automated builder and database of protein/membrane complexes for molecular dynamics simulations. PLoS One 2, e880–1–e880–9. [PubMed: 17849009]

(23). Wells DB, Bhattacharya S, Carr R, Maffeo C, Ho A, Comer J and Aksimentiev A (2012) Optimization of the molecular dynamics method for simulations of DNA and ion transport through biological nanopores, in Nanopore-Based Technology (Gracheva ME, Ed.) pp 165–186; Humana Press, New York.

(24). Steinbach PJ, and Brooks BR (1994) New spherical-cutoff methods for long-range forces in macromolecular simulation. J. Comput. Chem 15, 667–683.

(25). Essmann U, Perera L, Berkowitz ML, Darden T, Lee H, and Pedersen LG (1995) A smooth particle mesh Ewald method. J. Chem. Phys 103, 8577–8593.

(26). Barth E, Kuczera K, Leimkuhler B, and Skeel RD (1995) Algorithms for constrained molecular-dynamics. J. Comput. Chem 16, 1192–1209.

(27). Bhattacharya S, Muzard J, Payet L, Mathe J, Bockelmann U, Aksimentiev A, and Viasnoff V (2011) Rectification of the current in alpha-hemolysin pore depends on the cation type: The alkali series probed by molecular dynamics simulations and experiments. J. Phys. Chem C 115, 4255–4264.

(28). Cruz-Chu ER, Aksimentiev A, and Schulten K (2009) Ionic current rectification through silica nanopores. J. Phys. Chem C 113, 1850–1862.

(29). Maffeo C, Bhattacharya S, Yoo J, Wells D, and Aksimentiev A (2012) Modeling and simulation of ion channels. Chem. Rev 112, 6250–6284. [PubMed: 23035940]

(30). Aksimentiev A (2010) Deciphering ionic current signatures of DNA transport through a nanopore. Nanoscale 2, 468–483. [PubMed: 20644747]

(31). Jensen MO, Borhani DW, Lindorff-Larsen K, Maragakis P, Jogini V, Eastwood MP, Dror RO, and Shaw DE (2010) Principles of conduction and hydrophobic gating in K+ channels. Proc. Natl. Acad. Sci. U.S.A 107, 5833–5838. [PubMed: 20231479]

(32). Jensen MO, Jogini V, Eastwood MP, and Shaw DE (2013) Atomic-level simulation of current-voltage relationships in single-file ion channels. J. Gen. Physiol 141, 619–632. [PubMed: 23589581]

(33). Phillips JC, Braun R, Wang W, Gumbart J, Tajkhorshid E, Villa E, Chipot C, Skeel RD, Kalé L, and Schulten K (2005) Scalable molecular dynamics with NAMD. J. Comput. Biol 26, 1781–1802.

(34). Brooks BR, Brooks CL 3rd, Mackerell AD Jr., Nilsson L, Petrella RJ, Roux B, Won Y, Archontis G, Bartels C, Boresch S, Caflisch A, Caves L, Cui Q, Dinner AR, Feig M, Fischer S, Gao J, Hodoscek M, Im W, Kuczera K, Lazaridis T, Ma J, Ovchinnikov V, Paci E, Pastor RW, Post CB, Pu JZ, Schaefer M, Tidor B, Venable RM, Woodcock HL, Wu X, Yang W, York DM, and Karplus M (2009) CHARMM: The biomolecular simulation program. J. Comput. Chem 30, 1545–1614. [PubMed: 19444816]

(35). Klauda JB, Venable RM, Freites JA, O'Connor JW, Tobias DJ, Mondragon-Ramirez C, Vorobyov I, MacKerell AD, and Pastor RW (2010) Update of the CHARMM all-atom additive force field for lipids: Validation on six lipid types. J. Phys. Chem. B 114, 7830–7843. [PubMed: 20496934]

(36). Jorgensen WL, Chandrasekhar J, Madura JD, Impey RW, and Klein ML (1983) Comparison of simple potential functions for simulating liquid water. J. Chem. Phys 79, 926–935.

(37). Chaudhury S, Berrondo M, Weitzner BD, Muthu P, Bergman H, and Gray JJ (2011) Benchmarking and analysis of protein docking performance in Rosetta v3.2. PLoS One 6, e22477–1–e22477–13. [PubMed: 21829626]

(38). Wang C, Bradley P, and Baker D (2007) Protein-protein docking with backbone flexibility. J. Mol. Biol 373, 503–519. [PubMed: 17825317]

(39). Kumar S, Huang C, Zheng G, Bohm E, Bhatele A, Phillips JC, Yu H, and Kale LV (2008) Scalable molecular dynamics with NAMD on the IBM blue gene/L system. IBM J. Res. Dev 52, 177–188.

(40). Chipot C (2013) Frontiers in free energy calculations of biological systems. WIREs Comput. Mol. Sci [Online early access] DOI: 10.1002/wcms.1157. Published Online: June 6, 2013.

(41). Schlitter J, Engels M, Kruger P, Jacoby E, and Wollmer A (1993) Targeted molecular-dynamics simulation of conformational change – application to the T↔R transition in insulin. Mol. Simul 10, 291–296.

(42). Zhao CF, and Noskov SY (2013) The molecular mechanism of ion-dependent gating in secondary transporters. PLoS Comp. Biol 9, e1003296–1–e1003296–12.

(43). Roux B (1995) The calculation of the potential of mean force using computer-simulations. Comput. Phys. Commun 91, 275–282.

(44). Allen TW, Andersen OS, and Roux B (2004) Energetics of ion conduction through the gramicidin channel. Proc. Natl. Acad. Sci. U.S.A 101, 117–122. [PubMed: 14691245]

(45). Kim I, and Allen TW (2011) On the selective ion binding hypothesis for potassium channels. Proc. Natl. Acad. Sci. U.S.A 108, 17963–17968. [PubMed: 22011574]

(46). Vorobyov I, Bennett WFD, Tieleman DP, Allen TW, and Noskov S (2012) The role of atomic polarization in the thermodynamics of chloroform partitioning to lipid bilayers. J. Chem. Theory Comput 8, 618–628. [PubMed: 26596610]

(47). Sasseville L, Cuervo JE, Lapointe JY, and Noskov SY (2011) The structural pathway for water permeation through sodium-glucose cotransporters. Biophys. J 101, 1887–1895. [PubMed: 22004742]

(48). Nina M, Beglov D, and Roux B (1997) Atomic radii for continuum electrostatics calculations based on molecular dynamics free energy simulations. J. Phys. Chem. B 101, 5239–5248.

(49). Jo S, Vargyas M, Vasko-Szedlar J, Roux B, and Im W (2008) PBEQ-Solver for online visualization of electrostatic potential of biomolecules. Nucleic Acids Res. 36, W270–W275. [PubMed: 18508808]

(50). Chanda B, Asamoah OK, Blunck R, Roux B, and Bezanilla F (2005) Gating charge displacement in voltage-gated ion channels involves limited transmembrane movement. Nature 436, 852–856. [PubMed: 16094369]

(51). Swanson JMJ, Henchman RH, and McCammon JA (2004) Revisiting free energy calculations: A theoretical connection to MM/PBSA and direct calculation of the association free energy. Biophys. J 86, 67–74. [PubMed: 14695250]

(52). Berneche S, and Roux B (2003) A microscopic view of ion conduction through the K+ channel. Proc. Natl. Acad. Sci. U.S.A 100, 8644–8648. [PubMed: 12837936]

(53). Gumbart JC, Roux B, and Chipot C (2013) Efficient determination of protein–protein standard binding free energies from first principles. J. Chem. Theory Comput 9, 3789–3798.

(54). Zhao CF, Caplan DA, and Noskov SY (2010) Evaluations of the absolute and relative free energies for antidepressant binding to the amino acid membrane transporter LeuT with free energy simulations. J. Chem. Theory Comput 6, 1900–1914. [PubMed: 26615849]

(55). Chen R, and Chung SH (2012) Binding modes of mu-conotoxin to the bacterial sodium channel (Na(v)Ab). Biophys. J 102, 483–488. [PubMed: 22325270]

(56). Choudhary OP, Ujwal R, Kowallis W, Coalson R, Abramson J, and Grabe M (2010) The electrostatics of VDAC: Implications for selectivity and gating. J. Mol. Biol 396, 580–592. [PubMed: 20005234]

(57). Bezrukov SM, Berezhkovski AM, Pustovoit MA, and Szabo A (2000) Particle number fluctuations in a membrane channel. J. Chem. Phys 113, 8206–8211.

(58). Berezhkovskii AM, Pustovoit MA, and Bezrukov SM (2002) Channel-facilitated membrane transport: Transit probability and interactions with the channel. J. Chem. Phys 116, 9952–9956.

(59). Berezhkovskii AM, and Bezrukov SM (2004) Optimizing transport of metabolites through large channels: Molecule sieves with and without binding. Biophys. J 88, L17–L19. [PubMed: 15626697]

(60). Rostovtseva TK, Gurnev PA, Chen MY, and Bezrukov SM (2012) Membrane lipid composition regulates tubulin interaction with mitochondrial voltage-dependent anion channel. J. Biol. Chem 287, 29589–29598. [PubMed: 22763701]

(61). Wang RY-R, Han Y, Krassovsky K, Sheffler W, Tyka M, and Baker D (2011) Modeling disordered regions in proteins using Rosetta. PLoS One 6, e22060–1–e22060–9. [PubMed: 21829444]

(62). Aksimentiev A, and Schulten K (2005) Imaging the permeability of alpha-hemolysin with molecular dynamics. Biophys. J 88, 3745–3761. [PubMed: 15764651]

(63). Im W, and Roux B (2002) Ion permeation and selectivity of OmpF porin: A theoretical study based on molecular dynamics, brownian dynamics, and continuum electrodiffusion theory. J. Mol. Biol 322, 851–869. [PubMed: 12270719]

(64). Rui HA, Lee KI, Pastor RW, and Im W (2011) Molecular dynamics studies of ion permeation in VDAC. Biophys. J 100, 602–610. [PubMed: 21281574]

(65). Zachariae U, Schneider R, Briones R, Gattin Z, Demers JP, Giller K, Maier E, Zweckstetter M, Griesinger C, Becker S, Benz R, de Groot BL, and Lange A (2012) β-Barrel mobility underlies closure of the voltage-dependent anion channel. Structure 20, 1540–1549. [PubMed: 22841291]

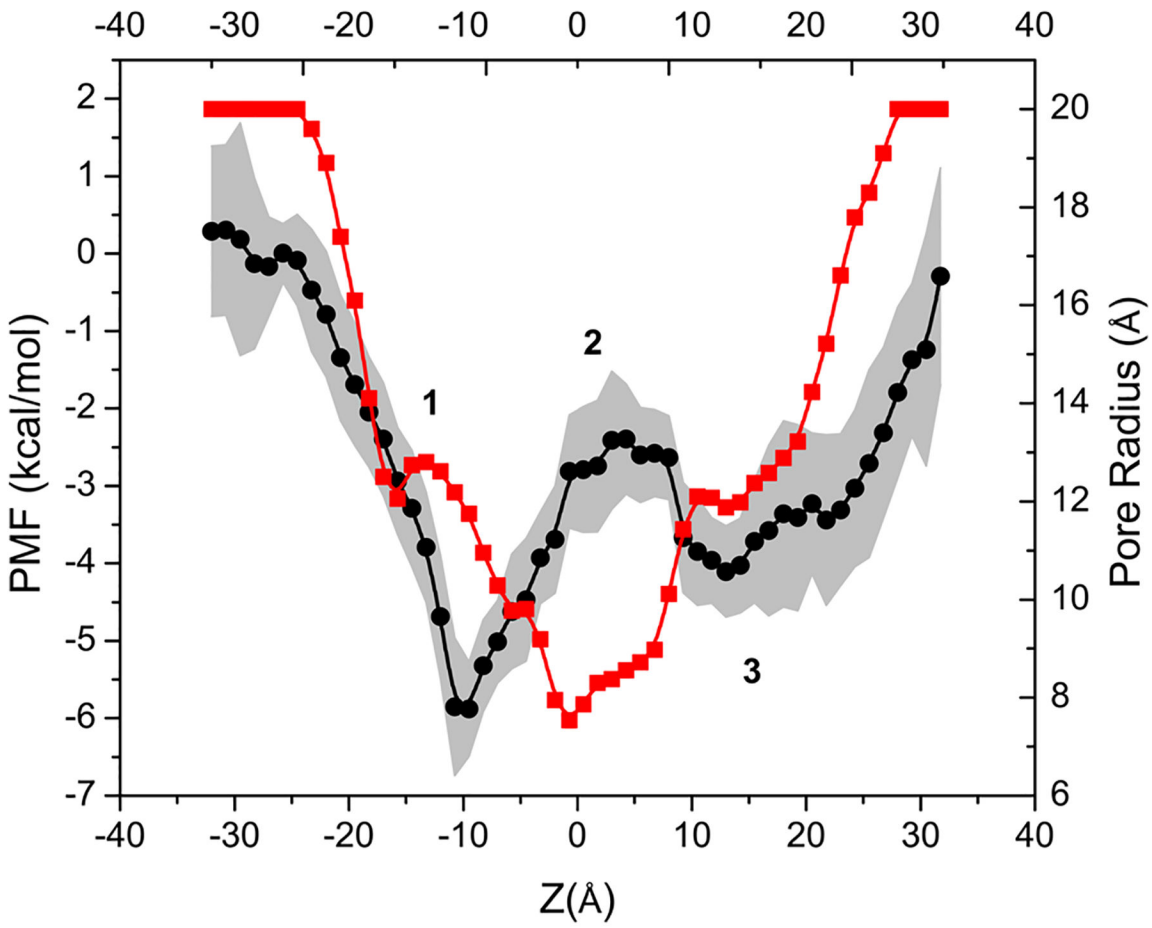

Figure 1.

Overlap of the potential of mean force (PMF) for ATP translocation across the VDAC1 pore (left *y* axis), with VDAC1 pore radius (right *y* axis) shown as solid black and red, respectively. The error bars were estimated from block averaging with seven blocks and are shown as the shadowed area. The high-affinity binding site, the barrier, and the lower-affinity site are labeled as states 1, 2, and 3, respectively. This notation is used in the text. Here and elsewhere, the *z* axis is the axis along the pore.

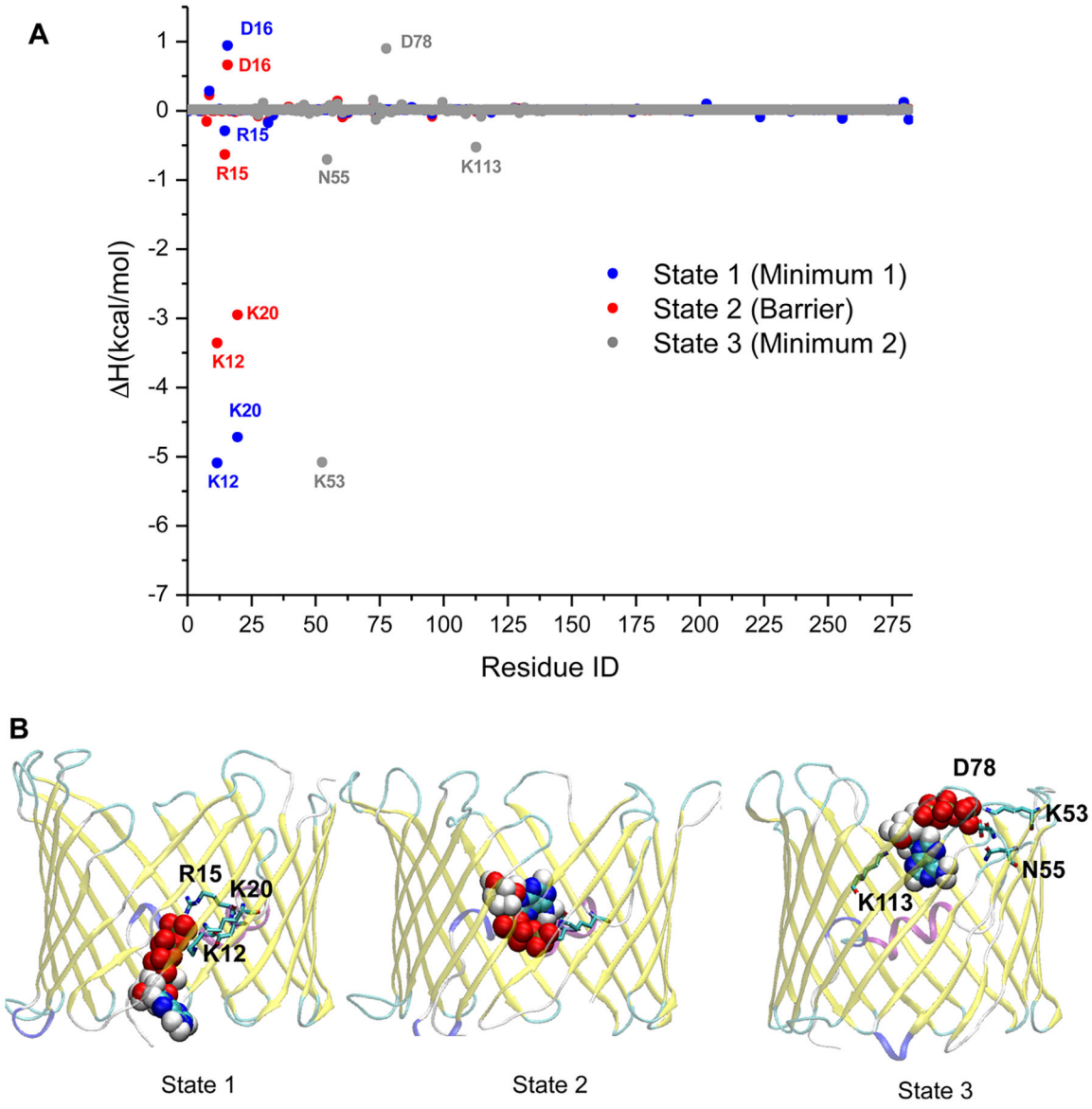

Figure 2.

(A) Per-residue decomposition of VDAC1-ATP binding free energy from MM-PBSA computations for states 1, 2, and 3 observed in the ATP translocation PMF (see Figure 1A). (B) Graphic representation of ATP coordination inside the VDAC1 pore in states 1, 2, and 3 with snapshots from the umbrella windows. ATP is shown in CPK representation, and the amino-acid residues forming binding pocket for states 1, 2, and 3 are shown as sticks.

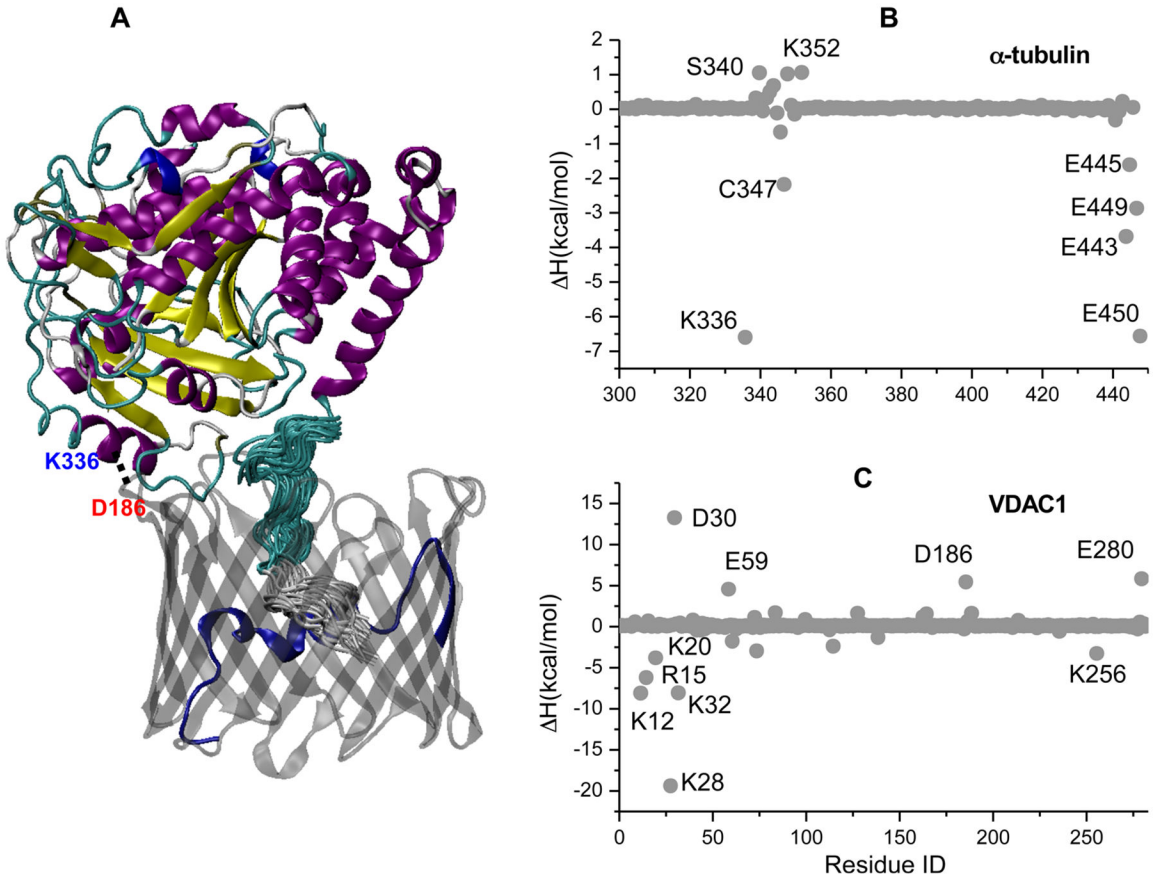

Figure 3.

(A) Molecular picture of the VDAC1–α-tubulin complex. The stable salt bridge between K336 of tubulin (shown in blue) and D186 of VDAC1 (shown in red) is illustrated by the dotted line. (B, C) Per-residue contributions to the VDAC–tubulin binding enthalpy for tubulin (B) and VDAC1 (C).

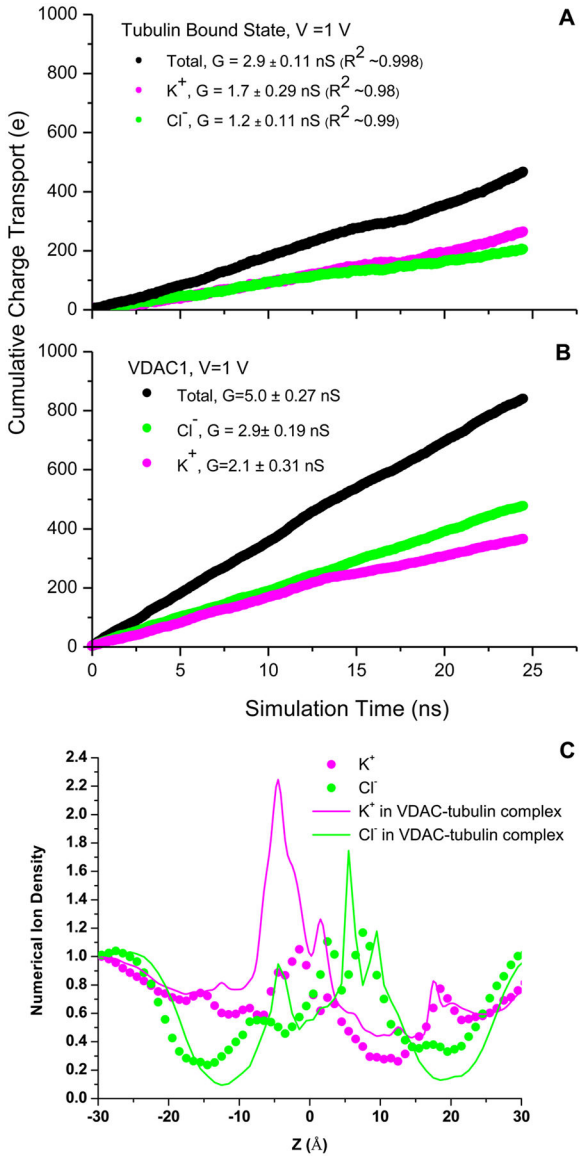

Figure 4.

Time series of cumulative charge transfer at $V = 1$ V and $C = 1$ M KCl for the tubulin-blocked (A) and tubulin-free (B) states of VDAC1. The cation component of the current is shown in magenta, and the anions contribution is shown in green. Total current is shown in black. (C) Number of K^+ and Cl^- ions across the channel for the tubulin-bound (solid lines) and tubulin-free (symbols) states.

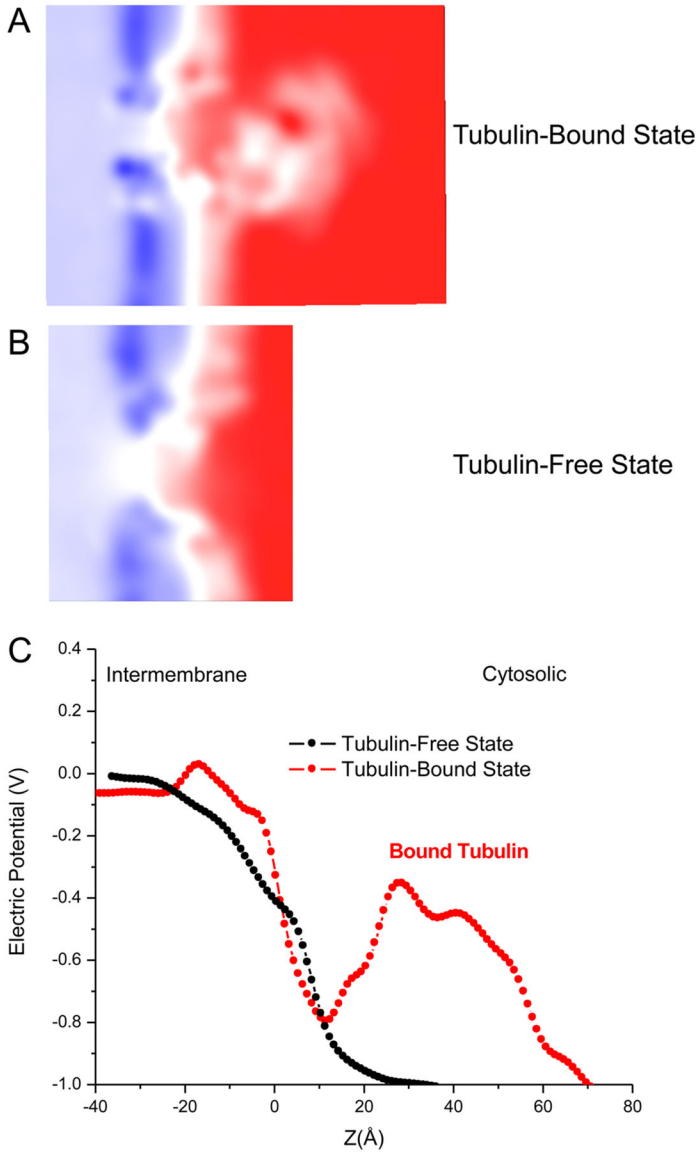

Figure 5.

(A, B) Cut-through of the electrostatic potential along the *z* axis for the VDAC1–tubulin (A) and VDAC1 (B) systems averaged over the last 50 ns of the MD simulations with the applied electric potential of $V = 1$ V. (C) Electrostatic potential along the *z* axis for VDAC (black symbols) and the VDAC–tubulin complex (red symbols). The membrane region is aligned for both systems.

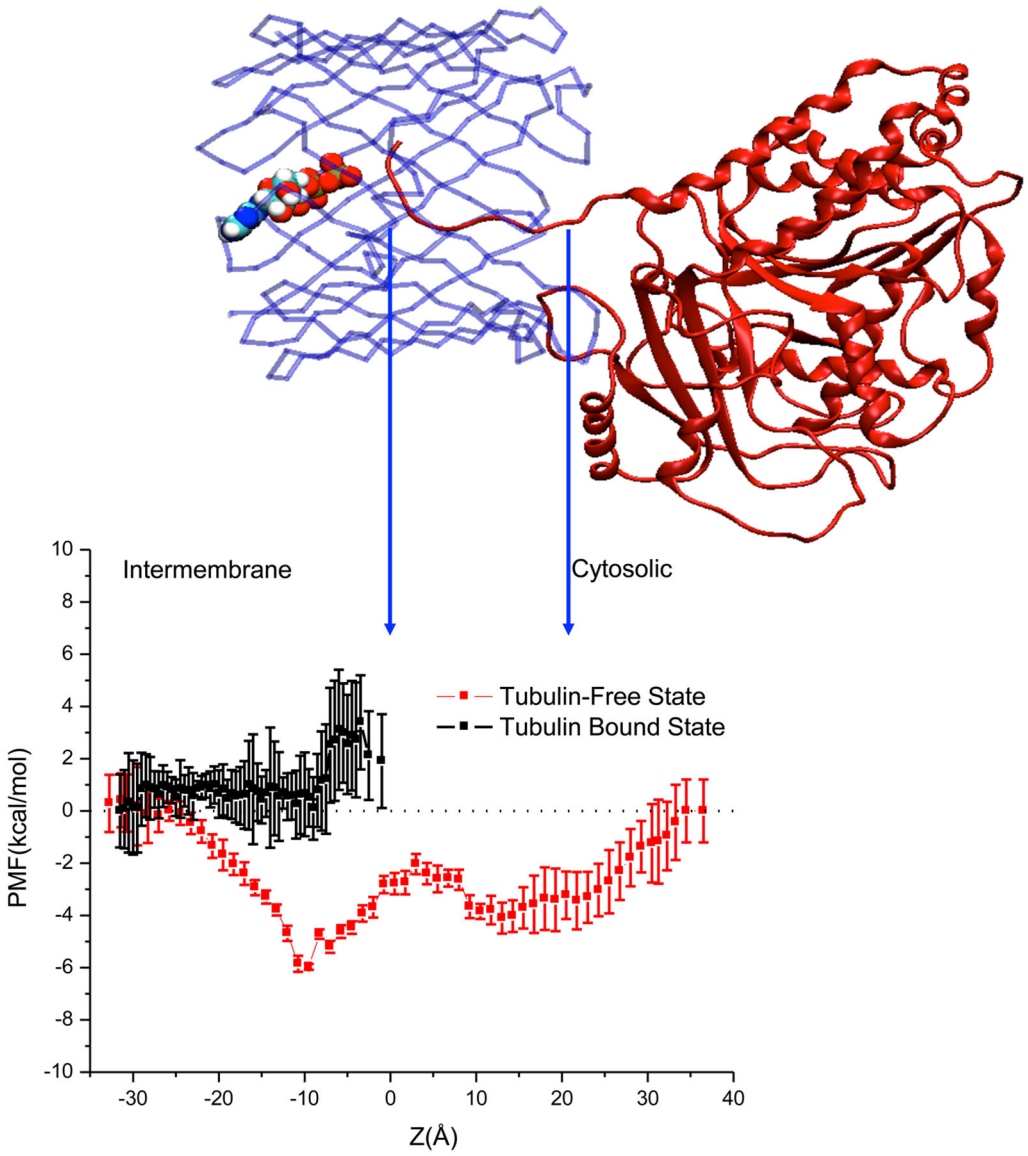

Figure 6.

Comparison of PMF profiles for ATP transport across the open and CTT-blocked VDAC1. The molecular structure of the VDAC–tubulin complex illustrates the depth of α-tubulin CTT penetration. The ATP molecule is shown in CPK. The presence of CTT bound to the VDAC pore makes the evaluation of the PMF section for $z > 0.0$ Å challenging because of steric penalties.